FINAL REPORT
U.S. Department of Energy

Particle Generation by Laser Ablation in Support of Chemical Analysis of High Level Mixed Waste from Plutonium Production Operations

Principal Investigator: J. Thomas Dickinson
Physics Department
Washington State University
Pullman, WA 99164-2814

Collaborator: Michael L. Alexander
EMSL K8-93
Pacific Northwest National Laboratory
P.O. Box 999
Richland, WA 99352

Project Number: 60075

Grant Number: DE-FG07-97ER62516

Grant Contracting Officer: Dallas Hoffer

Grant Project Officers: Ramoncita N. Massey
Matesh N. Varma

Project Duration: 15 September 1997–31 August 2001

November 30, 2001

Table of Contents

Executive Summary

We investigate particles produced by laser irradiation and their analysis by Laser Ablation Inductively Coupled Plasma Mass Spectroscopy (LA/ICP-MS), with a view towards optimizing particle production for analysis of high level waste materials and waste glass. LA/ICP-MS has considerable potential to increase the safety and speed of analysis required for the remediation of high level wastes from cold war plutonium production operations. In some sample types, notably the sodium nitrate-based wastes at Hanford and elsewhere, chemical analysis using typical laser conditions depends strongly on the details of sample history and composition in a complex fashion, rendering the results of analysis uncertain. Conversely, waste glass materials appear to be better behaved and require different strategies to optimize analysis.

Glass-based waste simulants have a relatively uniform composition and respond relatively consistently and predictably under high power laser radiation. Infrared lasers, such as the Nd-YAG laser at 1064 nm, generate copious quantities of fractured particles with relatively little melted material. Although the composition of these particles closely match the known sample composition, most of these particles are too large for efficient transport to and vaporization in the ICP-MS unit, and thus are not well suited for analysis. This is an important source of uncertainty in chemical analysis. Analytic uncertainties are reduced by using UV lasers at 355 nm, which produced large numbers of melted particles, and at 266-nm, where much of the particle mass was concentrated in nanometer-sized spheres. These nanoparticles are ideal for transport to and vaporization in the plasma torch. Although the composition of these particles differs significantly from the sample composition, these differences are consistent and reproducible. Best analytical results were obtained with particles generated in the UV. The change in particle generation mechanisms and thus particle size with laser frequency is accounted for by the deposition of laser energy in the near surface region of the sample. Laser absorption in the waste glass simulants (and in the anticipated waste glass material) increases

strongly as the laser wavelength decreases into the UV. This increased absorption results in higher surface temperatures and more melting and vaporization. This produces the small particles favored for transport to and vaporization in ICP-MS instrument.

Sodium nitrate based simulates were (as expected) much less tractable. We were unable to produce crystalline samples with uniform, significant dopant compositions. Variations in the particle composition can introduce unacceptable uncertainties into the analysis. Although the lack of doped crystalline samples with uniform compositions makes proof hard to obtain, it appears that the most reliable sample average results are obtained in the IR (1064 nm) with laser powers chosen to induce copious fracture without excessive melting. The choice of laser power represents a compromise between the ability to produce fracture and the need to avoid excessive melting. Laser powers that severely melt or vaporize the surface tend to produce particles severely depleted in elements like Cs, Ba, and Mg, whose ions are either much bigger or much smaller than Na; depletion is less severe for Sr, whose ionic radius more closely matches Na. The same features that render UV radiation preferable in the analysis of waste glass (more melting and vaporization) appear to be a liability in the analysis of nitrate-based wastes. This may in part be due to the low melting point and crystalline nature of sodium nitrate relative to typical waste glass materials. Nitrate fracture particles are generally larger than one would like for transport to and vaporization in the ICP-MS plasma. At this point, the large particle size does not seem to be an intractable problem, in part because nitrate-based particles are easier to vaporize than glass-based particles of the same size.

Research Objectives

Methods for compositional analysis of fissile materials and radioactive/toxic wastes are being developed to support characterization prior to treatment and remediation. Similar analysis is required to verify remediation efforts, e.g., to assure that the composition of glass-matrix waste forms falls within acceptable limits. The need for rapid, real-time, on site characterization of waste at DOE sites has led to deployment of laser ablation-inductively coupled plasma mass spectroscopy (LA/ICP-MS) systems for elemental and isotopic analysis at several locations, including Hanford, Los Alamos, and INEEL. These systems can provide qualitative or semi-quantitative analysis of certain sample types with minimal sample handling. Research into the fundamental physical processes of particle formation during laser ablation is required to provide basic understanding that will allow us to maximize the utility of these systems. A major consideration is the presence of non-metallic, crystalline, polycrystalline, and amorphous, wide bandgap materials or oxide films. This collaboration combined fundamental studies of mechanisms to provide underlying scientific insight into the relevant parameters influencing particle production, particle properties, and factors relating directly to glove-box installed ICP-MS analysis of both simulants and actual radioactive and toxic waste.

Our work focused on (1) ablation mechanisms and (2) the effect of the physical and chemical state of the sample (e.g., impurity concentration, particle morphology, and defect concentration) on the character of the particles produced by laser ablation. We examined the solid and condensed state properties of the sample, the coupling to the laser beam, and the dynamic electronic, physical, and chemical processes which ultimately generate the particles that are entrained and delivered to a distant ICP unit. This required careful examination of the intermediate steps such as formation of sub-micron to micron sized particles.

Our research included studies of the following:

- The absorption mechanisms and the role of laser parameters (wavelength, pulse width, fluence) in coupling energy into the solid.
- Characterization of the chemical and physical nature of the ejected particles (using several spectroscopies and microscopies).
- The consequences of aggregation and vapor deposition on the particle.
- The role of sample morphology and physical state on particle formation and stoichiometry.
- The formation mechanisms and morphology and composition of laser produced particles including gas phase aggregation and chemistry.

In general, these studies directly support other methods where are used, e.g., the production of plume fluorescence for spectral analysis, vaporization for direct mass analysis, as well as vaporization and particle formation for possible capture by various charged particle traps.

Methods and Results

Physical Characterization of $NaNO_3$ Particles.[1,2] Single crystal $NaNO_3$ was prepared by slowly cooling (1 °C/hour) molten material in a round-bottom flask. Single, 7-ns pulses of a Nd:YAG laser (Continuum Surelight II) were focused (without aperture) onto samples cleaved from the boule, and the resulting particles were collected on polished silicon substrates. Prior to exposure, some samples were polished using a damp piece of paper as a polishing cloth.

High resolution images of the collected particles were recorded with a LEO 982 field emission SEM at Pacific Northwest Laboratory's Environmental Molecular Science Laboratory. Lower resolution images were recorded with a JEOL JSM-6400 SEM at Washington State University. Energy dispersive analysis (EDS) of the smaller particles was performed to confirm their composition, eliminating the possibility that potential contaminants (e.g., dust) were confused with laser-produced $NaNO_3$ particles.

To simulate the effect of particle transport, particles were transported through about 1 m of tubing (3.2 mm inner diameter) in flowing Ar (1 liter/min) and collected on gold-coated Whatman Nucleopore track-etch membrane filters with 0.1 μm pore diameters. These particles could generally be imaged with the field emission microscope without additional gold coating. Particles collected on filters included smaller particles (< 100 nm) that were seldom observed on substrates due to the inordinately long time for them to settle out of the atmosphere. Particle collection was performed during continuous laser exposure over about five minutes, corresponding to about 1500 laser pulses.

Crystalline $NaNO_3$ is highly transparent at 1.06 μm, strongly limiting the IR energy absorbed by the sample during irradiation. Under these conditions, the great majority of laser radiation passes cleanly through the sample. The small amount of radiation that is absorbed can still generate substantial stresses in the material. In this geometry, laser absorption produces radial stresses perpendicular to the laser beam. Bullough and Gilman calculated that tensile stresses produced by a short laser pulse with uniform intensity distribution ("flat topped" beam profile) diverge in the center of the laser spot as the "relation wave" propagates inward from the edge of the laser spot.[3] Further, these tensile stresses exceed the compressive stress in the irradiated material during the laser pulse over a substantial area—about 20% of the laser spot radius. At low fluences, this tensile stress will not be sufficient to fracture the bulk material. However, damaged regions of the crystal, especially cleavage steps, are especially vulnerable to such stresses and can fracture off.

Cleavage steps are especially vulnerable to laser-induced damage.[4] Even residual steps on mechano-chemically polished material can substantially lower the fluence required for damage.[5] In some materials, cleavage induced deformation produces laser-absorbing point defects along steps,[4,6] increasing the laser induced thermal stresses and producing fracture. Laser energy scattered of steps and their associated internal interfaces can also locally enhance the laser energy density and result in similar heating and fracture.[7]

Because fracture occurs at temperatures well below the melting point, the composition of particles produced by fracture is far less susceptible to changes induced by thermal effects than particles produced by spallation of a melted layer or by vapor condensation. The chief disadvantage of the method is a tendency to produce large particles. In practical analytic applications, the collection geometry can be arranged so that the largest particles settle out of the air stream. In preliminary work with crystalline $NaNO_3$ doped with Cs, single laser pulses produced enough particles in the appropriate size range for the detection of ppm levels of Cs.

Deeper understanding of the particle production process may allow for substantial improvements.

Laser-induced fracture along cleavage steps can produce cleavage particles of an appropriate size for ICP-MS analysis at fluences low enough to preclude target or particle melting. The threshold fluence for the onset of melt features on particle and target surface at 1064 nm appears to coincide with the onset of optical breakdown—which in air is accompanied by an audible crack. Particle aggregation during transport is observed, presumably due to electrostatically charged fragments.

At laser fluences above the threshold for optical breakdown, the target surface and the resulting particles show extensive melt features. Cleaved surfaces yield large melted droplets, possibly due to the melting and ejection of cleavage debris. Fractured particles are produced at higher fluences, but the surfaces of these particles are extensively melted. Extensive aggregation is observed, both among particles collected on substrates and particles transported under ICP-MS-like conditions. Nanometer-scale particles are also observed, often forming web-like aggregates during transport. These nanoparticles apparently form by condensation from vapor. Nanoparticles collected on filter membranes may have nucleated in air, but similar particles organized into halo structures around larger, melted particles on collection substrates appear to have nucleated on the substrate. The role of surfaces in nanoparticle nucleation is an interesting question for further study.

Chemical Characterization $NaNO_3$ Particles.[8] Single crystal $NaNO_3$ doped with $Sr(NO_3)_2$ (nominally 1-1000 ppm atom fraction) and $CsNO_3$ (nominally 100 ppm atom fraction) was prepared by slowly cooling (1 °C/hour) molten material in a round-bottom flask. Similar samples were doped with $Mg(NO_3)_2$, $Sr(NO_3)_2$, and $Ba(NO_3)_2$ in comparable concentrations. Samples were cleaved from the resulting boules and mounted on a soda lime glass microscope slide in a particle collection chamber equipped with a transparent quartz cover and a beam stop. A Continuum Surelight Nd:YAG laser provided 7 ns pulses of radiation at 1064 and 355 nm. Particles formed by laser irradiation were entrained in flowing argon and transported to a Fissons Instruments VG Plasma Quad PQ2+ STE ICP-MS unit. The MS detector was operated in the pulse counting mode. First, a standard waste glass sample (Composition Variability Study Numbers 19 or 16, denoted CVS19 or CVS16, respectively) was exposed to the laser for 120 s (6 mJ IR or 1.6 mJ UV) at the focal point of an $f = 100$ mm lens). ICP-MS analysis was performed at the cold "lab demo" system at PNNL. The hardware and software in this system are almost identical to those in the hot cell system at the Hanford site. Finally, the signal from the $NaNO_3$ sample was acquired for about 400 s, with the laser beam rastering over a 5×5 mm^2 square 2-4 times during data collection. Data were acquired under three conditions of laser exposure, chosen to provide appropriate particle densities at the ICP-MS.

An independent estimate of the number and size of particles produced by laser ablation was provided by sampling the Ar flow with a Particle Monitoring System Lasair 1001-(6) particle analyzer. This instrument utilizes scattered laser light to count particles in the 0.1-2.0 μm range.

ICP-MS and particle-size analysis under high power UV irradiation show strong incubation effects, often accompanying depletion of minority components. Relative to high and low power density IR particle production under UV irradiation is largely independent of local surface conditions, which is an advantage in many applications. High power IR exposure produces large amounts of particles and minimal incubation effects, but suffers extreme Cs-depletion. These disadvantages are overcome with low-power IR irradiation, which exploits

localized surface defects (cleavage steps) to produce particles by fracture. This sensitivity to surface condition results in strong point-to-point variations in particle production that can selectively sample regions with high impurity concentrations. It is possible that in highly structured solids such as saltcake waste, high densities of small structural features would allow for more consistent sampling of the surface by fracture at even lower power densities.

Given the compositional heterogeneity of our doped single crystals, the best comparisons between analytical results and expected sample compositions were obtained by rastering the laser beam completely across sample slices that extended completely across the boule and summing the total observed counts for each impurity component. Under these conditions, reasonable agreement was found (± 20%) with the expected impurity fractions for all impurities present at 100 atom ppm or more when a modest IR laser fluence (1064 nm, 2.5 mJ in a 100 μm diameter laser spot) was used to generate particles. Scan to scan reproducibility was about 30%. Strong deviations from expected sample composition were observed at higher IR power densities (6 mJ in a 100 μm diameter laser spot) and under UV laser irradiation. Lower IR power densities (250 mJ in a 2.3 mm diameter laser spot) produced localized fracture along cleavage steps; although the composition of the resulting particles presumably provide a good match to the parent material, the composition of material around cleavage steps can deviate significantly from the nearby sample composition. Nevertheless, the best scan to scan reproducibility was achieved with these low power densities. Laser conditions which generate fracture consistently across the entire sample while minimizing melting and vaporation by the laser (e.g., 2.5 mJ at 1064 nm in a 100 μm diameter spot) appear to be the best for chemical analysis of crystalline $NaNO_3$.

Particulates formed from waste glass simulant (PNNL).[9] Studies at PNNL focused on the characterization of particulates formed under conditions as close as possible to those encountered in the LA/ICP-MS system at the 222S hot cell facility in Hanford. This is facilitated by the use of a cold "lab demo" system at PNNL. The hardware and software in this system are almost identical to those in the hot cell system at the Hanford site. Two pulsed laser systems were used to study the effect of laser parameters such as energy density, pulse length, and wavelength on the particulates produced by the laser ablation process. A Continuum Shurelite laser produced 7 ns pulses at 1064, 532, 355 and 266 nm. Most of the work presented here employed pulse energies of 100-200 μJ/pulse, although pulse energies ranging from 20 μJ to 90 mJ were investigated. Picosecond laser pulses are generated by an ORION laser system that uses stimulated Raman pulse compression methods to produce pulses lengths of 20 picoseconds and 20 μJ-2 mJ in energy. The wavelengths are shifted slightly by the Raman process but are close to the YAG wavelengths. Laser ablation studies on glass samples typically used a lens with a focal length of 10 cm and produced a 50 μm laser spot at the sample, corresponding to an energy density of 5-10 J/cm^2. Longer focal length lenses of 30-40 cm were also used when investigating the production of particulates from laser ablation of sodium nitrate crystalline and salt cake samples. The laser pulse energy is monitored on-line using a beam splitter and a Molectron pulse energy meter. The beam profile was checked periodically using a CCD beam profiler to verify that no hot spots are present in the laser beam.

Samples are held in a quartz cylinder approximately 8 cm in diameter by 6 cm high with a window on the top for laser access. The bottom of the cylinder is open and is sealed to a Teflon base with an o-ring. The entire sample assembly is mounted on an X-Y-Z translation stage. A square raster pattern of 1–5 mm^2 is created by moving the sample continuously relative to the laser beam during data acquisition. Argon gas flows at 1 liter/minute into the lower part the sample cell and exits directly across the cell near the top. The gas flow created by this

geometry entrains the ablated sample material and transports it to the ICP-MS. The laser-ablated particle size distribution is monitored on-line by an isokinetic sampler connected to a Particle Measurement Systems (PMS) particle size analyzer. The PMS measures the number of particles present in eight size classes from 0.1–2 μm in diameter using laser light scattering. The particles are then carried into the ICP/MS through 10 meters of 0.125" (inner diameter) tubing. During some studies, a Nucleopore 0.1 μm filter was placed in-line to intercept particulates en route to the ICP-MS. These filters were then examined by a scanning electron microscope (SEM) and analyzed by energy dispersive x-ray spectroscopy (EDX) to characterize the size, shape, and composition of the ablated particles.

The primary types of samples studied for this EMSP project were vitrified waste (glass) simulants and sodium nitrate salt cake simulants. The glass sample used was Composition Variability Study #19 (CVS19), a relatively dark colored vitrified wasteform simulant. These were chosen due to their relevance to the cleanup efforts at the Hanford site. Work at PNNL during the first two years of this project was focused mainly on glass samples, motivated not only by the relevance to Hanford, but because the composition of vitrified material is more homogeneous than salt cake type samples. The inherent homogeneity allows variations in the LA/ICP-MS method to be separated from variations in the sample itself. Furthermore, optical and other physical properties are more uniform and well-defined for glass samples.

One of the first tasks undertaken during this project was to understand the underlying cause of the variation of the degree of precision with laser wavelength, specifically for glass samples. Improved understanding of this relationship has the potential to lead to improved results for all sample types. The on-line optical particle measurement system was used to determine the size distribution of particles under the same conditions.

Three classes of particulates were observed for ablation of CVC 19 under these laser conditions:

(1) large irregular, sharp-edged particles > 1 μm,
(2) smooth spherical or ovoid particles, and
(3) aggregates of many small (1 –50 nm) ultra-fine particles.

In glassy samples like CVS19, we can neglect thermal conduction on the timescale of the laser pulse. Therefore the laser heats a volume of the sample whose depth is determined by the optical density at the ablation wavelength. The optical density for CVS19 increases as the laser wavelength decreases, resulting in smaller absorption depths and irradiated volumes. The longest wavelengths heat the greatest volumes, resulting in lower surface temperatures for a given laser pulse energy.

At 1064 nm, a large amount of mass is ejected in the form of large, fractured chunks. These are consistent with a temperature high enough to thermally fracture the surface, but too low to completely melt the irradiated volume. Laser ablation at 532 nm displays intermediate behavior, with partially melted fracture particles. Finally, ablation at 355 and 266 nm respectively show only spherical particles, with no fracture particles. Large round particles may be spalled from the surface when the laser-induced shock wave reflects from the boundary between molten and solid material. At 266 nm, more material is observed in the form of small ultra-fine particles than at 355 nm. At 266 nm the absorption depth and the irradiated volume is the smallest. Thus near surface heating is able to vaporize more material. This vapor condenses as small particles, which then aggregate under the influence of electrostatic forces.

Energy dispersive x-ray spectrometry (EDX) in the SEM instrument was used to characterize the particle compositions. This technique is only good for major components, but does provide a valuable indication of which particulate fraction most closely represents the sample material. Samples were collected that represented the fracture, melt spallation and ultra-fine aggregate particles generated by the ablation process. Measurements were made for three different samples for each particle type as well as three different locations on the target sample.

The composition of the large fracture particles and the melt spalled particles are the closest to the original composition of the CVS19 glass sample. This is an interesting result in light of the earlier observation that UV ablation produces a majority of the particle mass as ultra-fine particles and yields the most reproducible analytical results. It suggests that the superior precision of the UV results is due to higher reliability in particle transport and processing in the ICP plasma. If fracture or melt particles can be reliably produced in a smaller size range, the capability of LA/ICP-MS for precise analysis can potentially be improved.

Relevance, Impact, and Technology Transfer

The current technology of choice for immobilizing high level nitrate-based wastes at Hanford involves incorporating this waste into a glassy matrix. The long term stability of waste glass matricies can be significantly degraded by the presence of certain impurities (e.g., Fe, P) at the one percent level. Heat generated by radioactive decay is a significant factor in waste storage, and the majority of heating is due to a few fission products remaining in the waste. Elemental and isotopic analysis of waste material being prepared for treatment can be a rate limiting step in waste processing. Inaccurate chemical analysis can greatly add to the cost of processing high level wastes in any scenario, and can render the product unable to meet remediation goals.

Laser ablation-inductively coupled plasma mass spectroscopy (LA/ICP-MS) systems for elemental and isotopic analysis have been deployed at several locations, including Hanford, Los Alamos, and INEEL. These systems can provide qualitative or semi-quantitative analysis of certain sample types with minimal sample handling. Our collaborators in this work, Michael Alexander and Albert Mendoza of Pacific Northwest National Laboratories, share responsibility for a lab demonstration LA/ICP-MS system used to develop and test methods prior to deployment in an actual radiological environment. In particular, Albert Mendoza and Steve Langford of WSU developed procedures in PNNL's LA/ICP-MS instrument in the Stevens Drive facility. The hardware and software in this system are almost identical to those in the 222S hot cell system at the Hanford site, and is often shared with Hanford staff who use hot cell LA/ICP-MS. Thus the technology developed in this work is available to PNNL staff, and can be transmitted to the staff directly responsible for analysis of radiological materials on an as-needed basis.

The actual implementation of LA/ICP-MS analysis will depend on part on the final arrangements for waste remediation, which we understand are incomplete. Efforts to subcontract waste remediation to a civilian contractor in principle remove Hanford staff from direct responsibility for routine chemical analysis. Waste analysis by Hanford staff will still be required on an occasional basis, and LA/ICP-MS will remain an attractive option for any entity that contracts to manufacture waste glass. An understanding of the particle formation process should decrease the costs and increase the safety of this work.

Project Productivity

A major unfulfilled goal in this work was the preparation of doped, single crystal sodium nitrate samples with known, uniform distributions of impurity components. This in turn made it impossible to compare the particle stoichiometry relative to the original sample material, except on an average basis. This is an important item for future work.

Personnel Supported

Post-doctoral Associates:	Stephen Langford, WSU. Albert Mendoza, PNL. Doug Weir, PNL.
Undergraduates:	Amanda Hedges, PNL. Jackson Davis, PNL.

Publications

Mechanisms of laser desorption of positive ions and plume formation in ionic crystals: J. T. Dickinson, D. R. Ermer, J.-J. Shin, and S. C. Langford, *Appl. Surf. Sci.* 127-129, 7-20 (1998).

Pulsed laser positive ion desorption from a model hydrated inorganic crystal ($CaHPO_4 \cdot 2H_2O$) at 248 nm: M. L. Dawes, S. C. Langford, and J. T. Dickinson, *Appl. Surf. Sci.* 127-129, 81-87 (1998).

Electrostatic expansion of a tenuous plasma produced by excimer laser-irradiation of MgO: D. R. Ermer, S. C. Langford, and J. T. Dickinson, *Appl. Surf. Sci.* 127-129, 977-982 (1998).

Photoelectron emission studies of cleaved and excimer laser irradiated single crystal surfaces of $NaNO_3$ and $NaNO_2$: C. Bandis, L. Scudiero, S. C. Langford, and J. T. Dickinson, *Surf. Sci.* 443(3), 413-419 (1999).

Laser desorption of energetic sodium ions from single-crystal $NaNO_3$ at 1064 nm: C. Bandis, S. C. Langford, J. T. Dickinson, and D. R. Ermer, *Appl. Phys. A* 69, S129-S132 (1999).

The production of sub-micron sodium nitrate particles by laser ablation: S. C. Langford, J. T. Dickinson, and M. L. Alexander, Appl. Phys. A 69, S647-S650 (1999).

Effect of heat treatment on UV laser induced positive ion desorption in $CaHPO_4 \cdot 2H_2O$: Y. Kawaguchi, M. L. Dawes, S. C. Langford, and J. T. Dickinson, *Appl. Phys. A* 69, S621-S624 (1999).

Consequences of combining laser irradiation with other stimuli on laser desorption and ablation from wide bandgap insulators, J. T. Dickinson, S. C. Langford, C. Bandis, M. L. Dawes, and Y. Kawaguchi, *Appl. Surf. Sci.* 154, 291-304 (2000).

Laser induced electron and sodium ion emission from single crystal $NaNO_3$ at 1064 nm, C. Bandis, S. C. Langford, J. T. Dickinson, D. R. Ermer, Norioki Itoh, *J. Appl. Phys.* 87(3), 1522-1528 (2000).

Desorption of positive ions from ionic crystals accompanying 248 nm laser irradiation, C. Bandis, S. C. Langford, J. T. Dickinson, *Appl. Phys. Lett.* 76(4), 421-423 (2000).

Interaction of wide band gap single crystals with 248 nm laser irradiation. VI. The influence of thermal pre-treatment on laser desorption of positive ions from a water-containing ionic crystal ($CaHPO_4 \cdot 2H_2O$): Y. Kawaguchi, M. L. Dawes, S. C. Langford, and J. T. Dickinson, *J. Appl. Phys.* 88(2), 647-646 (2000).

Investigations of laser desorption from modified surfaces of ionic single crystals: C. Bandis, M. L. Dawes, Y. Kawaguchi, S. C. Langford, and J. T. Dickinson, to appear in *Laser*

Applications in Microelectronic and Optoelectronic Manufacturing, SPIE Proceedings Volume 3933, edited by H. Helvajian, K. Sugioka, M. C. Gower and J. J. Dubowski (2000).

Interaction of wide band gap single crystals with 248 nm laser irradiation. VII. Localized plasma formation on NaCl single crystal surfaces, Y. Kawaguchi, M. L. Dawes, S. C. Langford, and J. T. Dickinson, to appear in *J. Appl. Phys.* 89(4), (2001).

Interaction of wide band gap single crystals with 248 nm laser irradiation. VIII. Laser desorption of molecular ions from MgO: S. Kano, S. C. Langford, and J. T. Dickinson, to appear in *J. Appl. Phys.* 89(5), (2001).

Manuscripts in preparation

Matrix effects in the analysis of doped single crystal $NaNO_3$ by laser ablation inductively couple plasma mass spectroscopy: S. C. Langford and J. T. Dickinson, A. Mendoza and M. L. Alexander.

Laser-induced particle production from single crystal $NaNO_3$ at 1.06 μm: S. C. Langford, M. L. Alexander, and J. T. Dickinson.

Mechanisms of particle generation in laser ablation of solid materials for inductively coupled plasma mass spectrometer (ICP/MS), Michael L. Alexander, Albert Mendoza, and Amanda L. Hedges, J. Thomas Dickinson and Stephen C. Langford.

Interactions

Ejection of droplets and fractured particles from single crystal $NaNO_3$ during pulsed laser irradiation (poster): J. T. Dickinson, S. C. Langford, and M. L. Alexander, Gordon Research Conference on Laser Interactions with Materials, Proctor Academy, Andover, NH, June 10, 1998.

Particle generation by laser ablation in support of chemical analysis of high level mixed waste (poster): J. T. Dickinson, M. L. Alexander, and S. C. Langford, EMSP National Workshop, Chicago, IL, July 27-30, 1998.

Pulsed laser generated particulates from inorganic single crystals relevant to ICP-MS: J. T. Dickinson, S. C. Langford, and M. L. Alexander, 44th International Meeting of the Federation of Analytical Chemistry and Spectroscopy Societies, Austin, TX, USA, October 29, 1998.

Fundamental mechanisms of particulate formation by laser ablation for inductively coupled plasma mass spectrometry (LA/ICP-MS): M. L. Alexander, S. C. Langford and J. T. Dickinson, SPIE Photonics East, Boston, MA, November, 1998.

Fundamental mechanisms of particulate formation by laser ablation for inductively coupled plasma mass spectrometry (LA/ICP-MS) (invited): M. L. Alexander, S. C. Langford and J. T. Dickinson, CMST/EMSP workshop, Gaithersburg, MD, March 8-11, 1999.

Investigation of particle formation by laser ablation for elemental analysis by ICP/MS (student poster): Amanda L. Hedges, A. Mendoza and M. L. Alexander, American Chemical Society Spring 1999 Meeting.

The use of lasers in chemical analysis of toxic materials: J. Thomas Dickinson, Paul Scherrer Institute, Villigen PSI, Switzerland, June, 1999.

Laser desorption and chemical analysis: J. Thomas Dickinson, Physikalisch-Chemisches Institut, Ruprecht-Karls-Universität, Heidelberg, June, 1999.

The production of sub-micron sodium nitrate particles by laser ablation (poster): S. C. Langford, J. T. Dickinson, and M. L. Alexander, Conference on Laser Ablation: COLA 99, Göttingen, Germany, July 19-23, 1999.

Mechanisms of macro-particle formation in laser ablation sampling for chemical analysis: M. L. Alexander, Amanda L. Hedges, Albert Mendoza, S. C. Langford and J. T. Dickinson, Conference on Laser Ablation (COLA), Goettingen, Germany, July 19-23, 1999

Mechanisms of particulate formation by laser ablation of solid samples for chemical analysis by ICP/MS: Michael L. Alexander, Amanda L. Hedges, S. C. Langford and J. T. Dickinson, Annual Meeting of the Federation of Analytical Chemistry and Spectroscopy Societies, Vancouver, B. C., October 25-29, 1999.

Particle generation by laser ablation: M. L. Alexander, J. T. Dickinson, A. Mendoza, and S. C. Langford, EMPS National Workshop, Atlanta, GA, April 24-28, 2000.

Future Work

This work has opened up some promising leads and some important questions are yet to be resolved. Formally, this work will be continued by our PNNL collaborator with funding from a recently funded proposal entitled:

Validation and Method Development to Allow Routine Analysis of DOE Waste Forms by Laser Ablation Inductively Coupled Plasma Mass Spectrometry (LA/ICP/MS)

By Michael L. Alexander, John Hartman, Monty R. Smith—PNNL,

in response to a call from the National Energy Technology Laboratory for the US Department of Energy, "Environmental Management Applied Research."

Certain aspects of this work will be continued in the course of our research on laser ablation in ionic materials, which is funded in part by the DOE Office of Science under an ongoing grant entitled

UV Laser-Surface Interactions Relevant to Analytic Spectroscopy of Wide Band Gap Materials

J. Thomas Dickinson, WSU.

Issues to be addressed include:

- The production of smaller fracture particles by laser ablation, or procedures to prevent truly large particles from entering the ICP-MS plasma torch. Initial work with cyclone particle separators is promising.

- Nitrate-based standards for improved evaluation and calibration of LA/ICP-MS techniques. For instance, homogeneity might be improved by rapid solidification of doped melts.

- Work with more realistic nitrate-based waste simulants. Ease of analysis may influence the choice of waste form.

Issues for other workers include statistical methods to insure that the size and distribution of analyzed portions of the sample are sufficient to adequately represent the average composition of heterogeneous samples.

Appendix 1

Production of particles by laser-induced fracture of single crystal $NaNO_3$ for chemical analysis by inductively coupled mass spectroscopy (draft)

S. C. Langford,* M. L. Alexander†, James S. Young†, and J. T. Dickinson*

*Physics Department, Washington State University, Pullman, WA 99164-2814
†Pacific Northwest Laboratory, P.O. Box 999, Richland, WA 99352

We show that sodium nitrate particles suitable for inductively coupled plasma mass spectroscopy (ICP-MS) can be produced by fracture of cleaved, single crystal, sodium nitrate under pulsed 1.06 μm laser irradiation. The laser fluence employed is somewhat below the threshold for optical surface damage, and therefore does not significantly melt the surface. Most particles are produce by fracture along previously existing cleavage steps. We compare these fracture particles with particles produce at fluences above the fluence threshold for optical breakdown, where extensive melting is observed. This is work is motivated by the expectation that the composition of unmelted fracture particles would be virtually identical with the bulk composition—a great advantage in the analysis of these materials by ICP-MS.

1. Introduction

The generation of particles by intense laser irradiation has important applications in chemical analysis. In the case of inductively couple plasma mass spectroscopy (ICP-MS), laser-generated particles can often be analyzed directly, without intermediate wet chemical processes. The resulting reduction in sample handling and wastes volume can significantly improve the safety and cost of analyzing hazardous wastes. Solid sampling also facilitates the analysis of small regions in inhomogeneous samples (e.g., mineral grains in geologic samples), yielding information on the range of compositions rather than just the average composition. Understanding the particle generation mechanisms must be understood for these applications.[10-13]

In this work, we examine particle production during the exposure of single crystal $NaNO_3$ to pulsed Nd:YAG laser radiation (1.06 μm). Sodium nitrate is a major component of high level waste from cold war plutonium production operations. In some facilities, chemical analysis is the rate limiting step in processing waste for long-term storage. The small sample sizes and minimal sample handling required by laser ablation ICP-MS are extremely attractive for the analysis of these wastes. Particles for analysis must be small enough for efficient transport and digestion in the ICP plasma torch. Ideally, they should also have the same composition as the target material. In low melting point materials like $NaNO_3$, particles produced by laser ablation can be significantly altered by poorly understood thermal effects.[10,12] Nitrate decomposition during laser ablation can also produce large amounts of refractory oxides and peroxides,[14] which are often difficult to digest in the ICP plasma torch and complicate analysis.

Many of the matrix affects associated with analysis of sodium nitrate based wastes could

be minimized if particle production were principally due to fracture. Laser-induce fracture is relatively inefficient in terms of particle production rates, but requires no melting or vaporization and inherently produces particles with the bulk composition. We show that suitably small particles can be generated by exposing cleaved, single crystal sodium nitrate to fluences that do not melt the crystal surface. The principle particle production mechanism under these conditions involves fracture along cleavage steps. Fluences where fracture dominates usually do not generate a plasma-shock wave in the atmosphere above the surface, and thus are somewhat below what is generally considered the fluence threshold for surface damage. We compare fracture particles generated at this low fluence with particles generated at somewhat higher fluences (above the threshold for optical damage), where even fracture-related particles show extensive surface melting. Possible strategies for efficient production and collection of fracture particles suitable for ICP-MS are discussed.

2. Experiment

Single crystal $NaNO_3$ was prepared by slowly cooling (1 °C/hour) molten material in a round-bottom flask. Single, 7-ns pulses of a Nd:YAG laser (Continuum Surelight II) were focused (without aperture) onto samples cleaved from the boule, and the resulting particles were collected on polished silicon or copper substrates. The geometry for particle generation and collection is illustrated in Fig. 1. Prior to exposure, some samples were polished using a damp piece of paper as a polishing cloth. Care was taken to isolate the substrates from particles generated by sample handling.

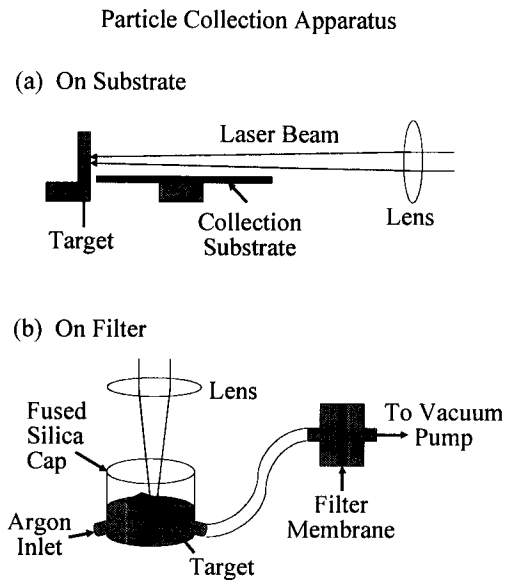

Fig. 1. Diagram of particle collection apparatus (a) for collection on a silicon substrate and (b) for collection on a filter membrane (100 nm pores).

High resolution images of the collected particles were recorded with a LEO 982 field emission SEM at Pacific Northwest Laboratory's Environmental Molecular Science Laboratory. Lower resolution images were recorded with a JEOL JSM-6400 SEM at Washington State University. Energy dispersive analysis (EDS) of the smaller particles was performed to confirm their composition, eliminating the possibility that potential contaminants (e.g., dust) were confused with laser-produced $NaNO_3$ particles.

To simulate the effect of particle transport, particles were transported through about 1 m of tubing (3.2 mm inner diameter) in flowing Ar (1 liter/min) and collected on gold-coated Whatman Nucleopore track-etch membrane filters with 0.1 μm pore diameters. These particles could generally be imaged with the field emission microscope without additional gold coating. Particles collected on filters included smaller particles (< 100 nm) that were seldom observed on substrates due to the inordinately long time for them to settle. Particle collection was performed during continuous laser exposure over about five minutes, corresponding to about 1500 laser pulses.

3. Results

Low fluences. A major change in particle production is observed near the threshold fluence for breakdown at the sample surface, about 4 J/cm^2 for the material used in this study under 1.06 μm irradiation in air. In air, optical breakdown is accompanied by an audible crack and is readily identified. HRSEM images of particles produced by a single laser pulse at a fluence of 3.4 J/cm^2, just below the breakdown threshold, are shown in Fig. 2. Figure 2(a) shows particles collected from a freshly cleaved target and Fig. 2(b) shows a comparable region of the substrate supporting an exposed, polished target. Although exposure of the cleaved target has produced a considerable amount of debris, no debris was observed on the substrate in front of the polished target.

The particles in Fig. 2(a) are strongly segregated by size, with smaller particles close to the target (upper right hand corner), and larger particles farther from the target. Smaller particles are strongly affected by viscous forces as they travel through the air and travel only small distances before coming to rest. Given a comparable initial horizontal velocity, larger particles travel further. For moving spherical particles in still air, the viscous reaction force on the particles is $F_v = 6\pi\eta Rv$, where η is the viscosity of air and R and v are the particle radius and velocity, respectively. Ignoring gravity, a particle with an initial velocity v_o parallel to the substrate will come to rest with respect to the surrounding air after traveling a distance d given by

$$d = \frac{2v_o \rho R^2}{9\eta} \tag{1}$$

where ρ is the particle density. Small particles will fall straight down to the substrate when their horizontal component of velocity falls to zero. Larger particles will hit the substrate before their horizontal component of velocity reaches zero. Thus d provides an upper bound on particle travel in still air.

Debris from Cleaved vs Polished $NaNO_3$
Exposed to a Single Pulse at 3.4 J/cm^2

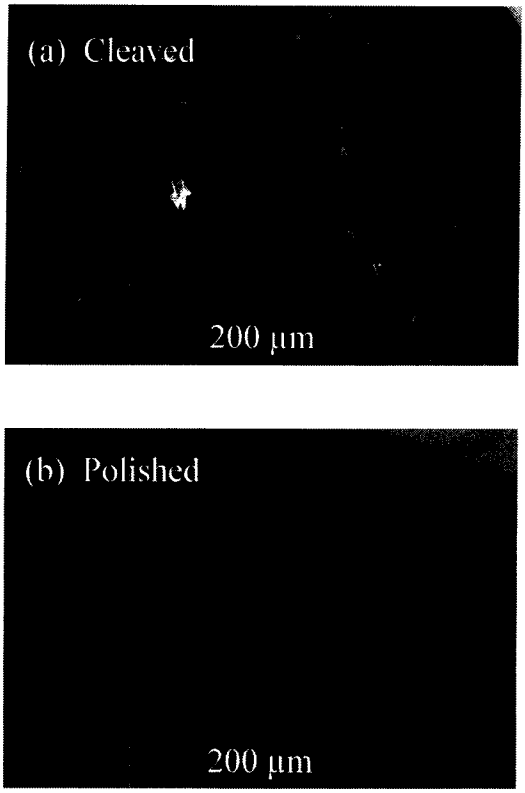

Fig. 2. Debris fields adjacent to $NaNO_3$ targets exposed to one pulse at a fluence of 3.5 J/cm^2 for (a) a freshly cleaved target and (b) a polished target. In each case, the target was positioned at the upper right hand of the image.

For sufficiently large particles, the effect of gravity on travel distance becomes significant. This sets an upper bound on the distance d, on the order of tens of cm for 250 μm particles. The largest particles observed on the substrates were platelike, with largest dimensions of about 50 μm some millimeters away from the target, so this maximum was not realized in this work. As noted below, particles collected on substrates were seldom as large as 10 μm across, suggesting that the largest particles produced by fracture are not transported efficiently.

Because few, if any, particles in this work are large enough to be seriously affected by gravity, the apparent sorting by particle size in Fig. 2(a) can be attributed to viscous drag in still air. In the presence of optical breakdown, the laser-induced shock wave produces air currents that hinder sorting, as noted below. Equation (1) can be used to estimate the average initial particle velocity, which is presumably be related to an initial particle velocity. Although the particles are not spherical, a significant number of particles 10 μm in diameter (R = 5 μm) appear to have fallen about 500 μm (d = 500 μm) from the surface. With ρ = 2.27 g/cm^3, and $\eta = 2 \times 10^{-5}$ g-cm^{-1}-s^{-1}, the average initial velocity is about 10 cm/s. This velocity is quite modest. Associating this velocity is imparted to the particles by the surface as the target expands under the laser beam, and that this may be associated with the fundamental longitudinal vibrational mode through the thickness of the sample, the associated peak strain at the surface is less than 1

$\times 10^{-6}$. If localized strains are responsible for the initial particle velocity, they would of course be much larger.

Due to the interest in particles suitable for ICP analysis, this work focused on particles under 2 μm in diameter. Such particles are readily entrained in a flowing gas, transported into a vacuum system, and digested in the flame of an ICP torch. A typical fracture particle is displayed in Fig. 3, showing the curved features characteristic of conchoidal (glass-like) fracture. This is a relatively high fracture energy mode for $NaNO_3$, but one that is expected during fracture at high strain rates. At low strain rates, pre-existing flaws grow slowly along low-energy paths (subcritical crack growth) until they reach the critical size required for fast crack growth (what we call failure). This critical size depends on flaw size and applied stress. When flaws have time to grow, failure occurs at lower stresses and crack growth is confined to low energy paths. At high strain rates, there is little time for flaws to grow and failure occurs at higher stresses, where the strain energy is sufficient to produce more complicated cracks. Even at high strain rates, crack growth eventually favors cleavage planes—and indeed many of the larger particles are distinctly rhombohedral.

Particles smaller than about 10 μm (in their longest dimension) are transported in large numbers for distances of some meters and are readily collected on filter membranes. An SEM image of a densely populated portion of a filter membrane appears in Fig. 4. By far the largest volume fraction is made up of particles 2-10 μm in their largest dimension. Particles of this size are generally difficult to digest in the plasma torch, although this difficulty is mitigated somewhat by their plate-like structure. With an average plate thickness of less than 2 μm, most of these particles have significantly less volume per unit surface area than spherical particles with the same maximum dimension. We have had some success in removing the larger particles with a cyclone particle separator placed in the argon line. These can be designed for relatively efficient removal of particles larger than 2 μm at gas flow rates employed in ICP-MS work.

Typical Particle from Cleaved $NaNO_3$
Exposed to a Single Pulse at 3.4 J/cm^2

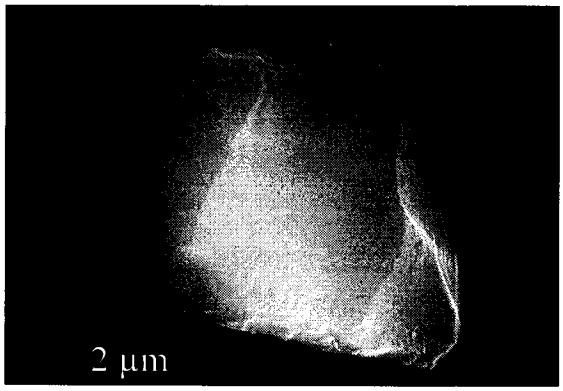

Fig. 3. Typical small particle from a cleaved target [the same target as in Fig. 2(a)] exposed to a single pulse at a fluence of 3.4 J/cm^2.

Particles Collected on Filter during IR Irradiation
at ~ 4 J/cm^2

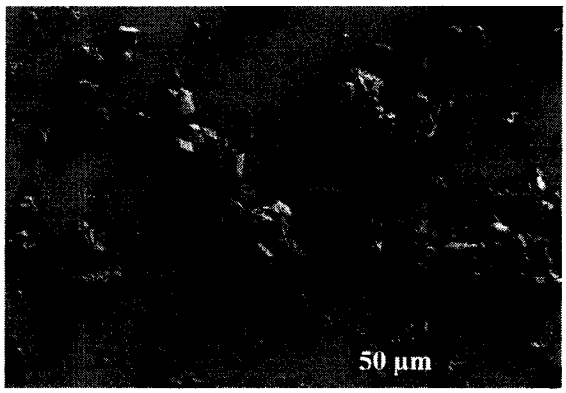

Fig. 4. Particles collected on a filter membrane during exposure to about 1500 laser pulses at a fluence of about 4 J/cm^2. Particle aggregation suggest that cleavage particles are electrostatically charged, either by cleavage or by laser exposure.

The large aggregates of particles observed in Fig. 4 presumably formed after transport to the membrane. The relatively small number of particles in this size range produced by single laser pulses [Fig. 2(a)] would strongly hinder aggregation during transport.

The virtual absence of particles from polished surfaces exposed to this fluence [Fig. 2(b)] strongly suggests that cleavage steps play an important role in particle production. This suggestion is confirmed by the presence of extensive damage along undercut cleavage steps on the cleaved sample. An SEM image of the target yielding the particles shown in Fig. 2(a) is shown in Fig. 5(a). Prior to laser exposure, cleavage steps curve smoothly across the surface. Fracture of undercut material along undercut steps which are not aligned with an easy cleavage direction produces a characteristic stair-step fracture pattern. This stair-step pattern is often the only visual indication of laser exposure at these fluences. Undercut steps are produced by unstable crack growth, where fingers of advancing crack extend ahead of the main crack front. These fingers seldom remain coplanar, and therefore produce a stepped surface, generally with many undercut terraces.[15] This process is virtually ubiquitous in the fracture of crystalline materials in the absence of heroic efforts to minimize it.

Undercut cleavage steps experience high strains immediately prior to ultimate failure, and tend to be highly deformed.[15] In previous work on single crystal MgO, the dislocations associated with this deformation interact strongly with UV laser irradiation.[6] At fluences just below the threshold for optical breakdown in MgO, UV laser radiation produces rows of holes similar to dislocation etch pits along many cleavage steps.[4] Evidence for similar features in single crystal $NaNO_3$ exposed to 1.06 μm laser irradiation is shown in Fig. 6(a). The staircase feature along this cleavage step was produced during the fracture of adjacent undercut material. Therefore we expect that most of the undercut material has been removed. The cleavage step geometry and the associated dislocations and pits following fracture of undercut material is indicated in Fig. 6(b). In MgO, we attributed hole formation to localized heating along dislocation cores. Dislocations are often favorable recombination sites for mobile charge (quasi-free electrons and holes from photo-ionized lattice defects);[16] heating by nonradiative recombination along the dislocation cores would vaporize material where the dislocation intersects the surface.[4]

High fluences. At higher fluences, laser irradiation consistently produces breakdown, yielding a distinct snap as the laser strikes the target. Particles produced under these conditions are far more likely to display melt-like features than at the lower fluences. In addition, the gas-phase shock wave significantly alters the distribution of the observed particles on the substrate.

Low-magnification views of collection substrates adjacent to cleaved and polished targets exposed to single pulses of 1.06 μm radiation at 5.0 J/cm^2 appear in Fig. 7. The substrate adjacent to the cleaved target shows a much lower particle density than the substrate for 3.4 J/cm^2 [Fig. 2(a)]. Further, the particles that remain are more poorly sorted with respect to size vs. distance from the target. Although some of this difference could be due to variations in the distribution of cleavage steps along the surface, the laser-induced shock wave appears to play a major role. The substrate adjacent to the polished surface shows two $NaNO_3$ particles in the field of view. As at 3.4 J/cm^2 polished target yields much fewer particles than the cleaved target. However, at 5.0 J/cm^2, the polished target does yield some particles, in contrast to the polished target at 3.4 J/cm^2. Both substrates displayed particles over large areas in front of their respective targets. In the case of the polished target, the observed particles were remarkably uniform in size.

Cleavage Steps on Single Crystal $NaNO_3$ Exposed to a Single Pulse at 3.4 J/cm^2

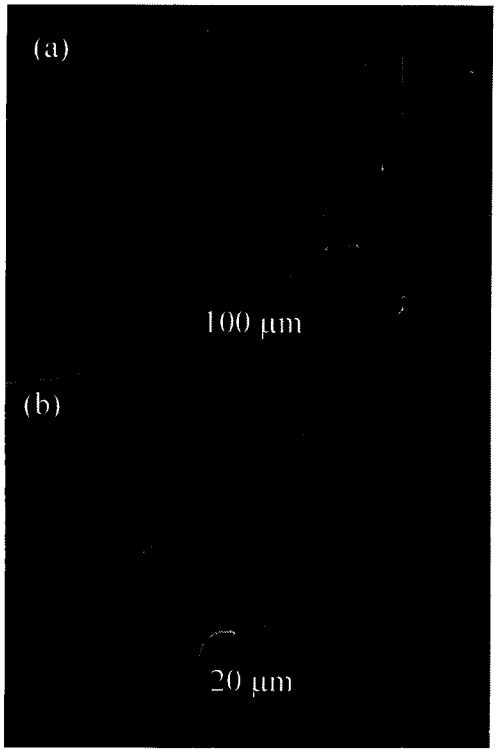

Fig. 5. Cleavage step fracture on $NaNO_3$ exposed to a single pulse at 3.4 J/cm^2. (a) Staircase fracture pattern characteristic of laser damage, and (b) magnified view of particles still attached to the cleavage step.

Holes along Step on $NaNO_3$ Surface Exposed to Single Pulse at 3.4 J/cm^2

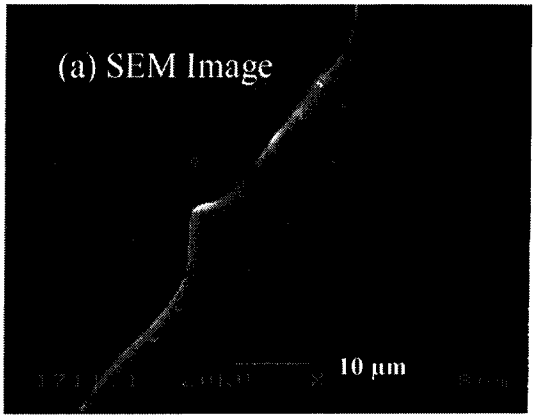

(b) Dislocation Configuration

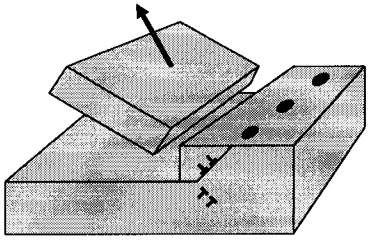

Fig. 6. (a) Magnified view of a fractured cleavage step exposed to a single pulse at 3.4 J/cm^2 and (b) diagram of undercut cleavage step following fracture showing dislocations at the crack tip similar to those thought to be responsible for the holes in (a). The holes would be produced by localized heating along the dislocation cores.

Typical particles from cleaved $NaNO_3$ at 5.0 J/cm^2 appear in Fig. 8. Many of these particles displayed small crystalline particles adhering to their surfaces—particles which presumably collided with and stuck to the larger parent particles in flight. Although some submicron-sized particles were observed, the longest dimension of most particles were on the order of a few microns—somewhat too large for easy transport to the ICP-MS. An important exception to this size distribution are the small particles forming a halo about the sphere in Fig. 8(b). These particles are typically a few hundred nanometers in diameter, and are almost always associated with a larger particle. Micron-sized particles landing a few millimeters from the target were much more likely to be accompanied by a halo than particles landing close to the target. In the case of plate-like particles, halos were often incomplete, localized near tips or edges which had experienced more melting than the rest of the plate.

Debris from Cleaved vs Polished $NaNO_3$
Exposed to a Single Pulse at 5.0 J/cm^2

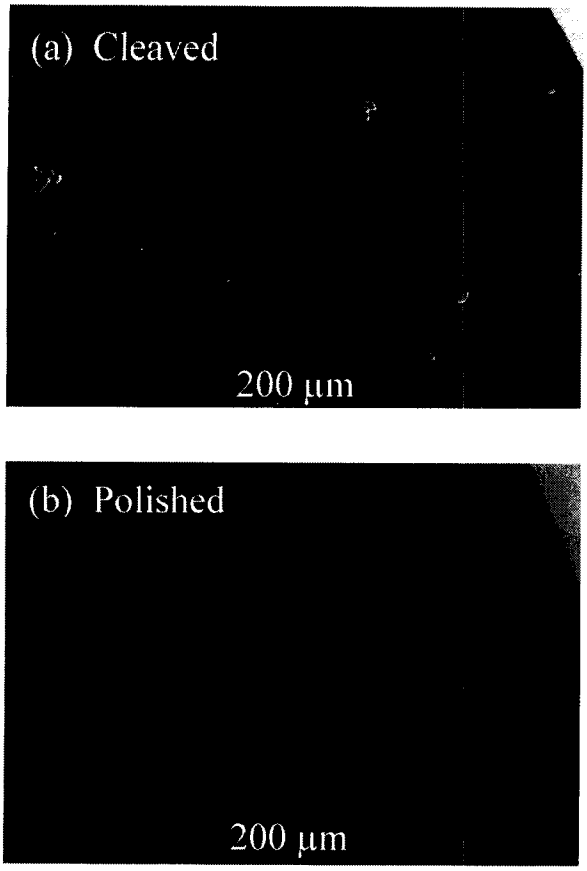

Fig. 7. Debris fields adjacent to $NaNO_3$ targets exposed to one pulse at a fluence of 5.0 J/cm^2 for (a) a freshly cleaved target and (b) a polished target. In each case, the target was positioned at the upper right hand of the image.

Particles from Cleaved $NaNO_3$
Exposed to a Single Pulse at 5.0 J/cm^2

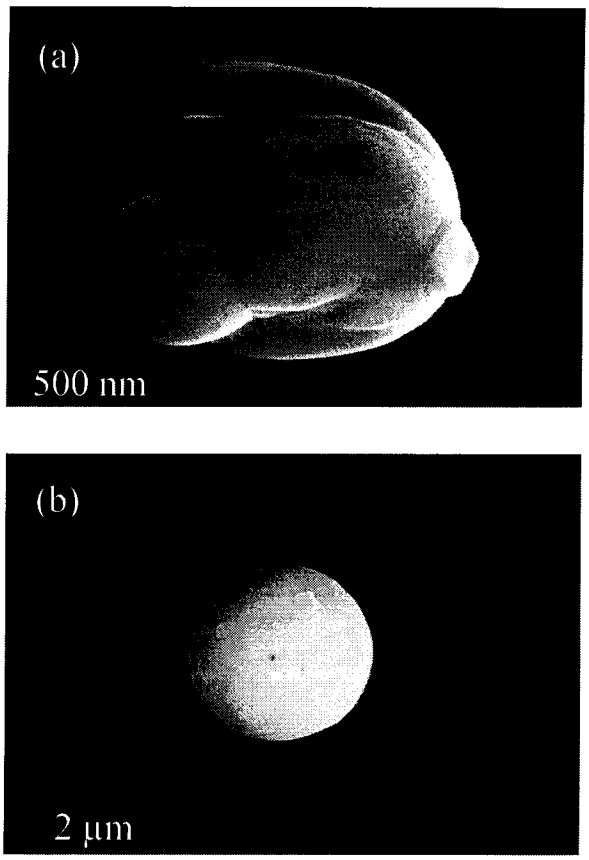

Fig. 8. Typical particles from a cleaved target [the same target as in Fig. 5(a)] exposed to a single pulse at a fluence of 5.0 J/cm^2: (a) a partially melted aggregate particle and (b) a melted sphere. We attribute the halo of nanoparticles around the sphere in (b) to nucleation and growth from $NaNO_3$ evaporated from the sphere and deposited on the substrate while the sphere was still molten.

As noted above, polished targets yield far fewer particles than cleaved targets. However, some particles are observed, and are distributed over a large area of the substrate. The particle imaged in Fig. 9 is typical of a number of strongly melted, plate-like particles with longest dimensions in the 5-10 μm range, more often than not accompanied by a halo of sub-micron particles. The polished targets yielded no melted spheres, suggesting that melted spheres from cleaved samples are formed when cleavage debris is melted by the laser. Cleavage debris may be especially vulnerable to melting due to high defect densities (and thus strong laser absorption) and poor thermal contact with the bulk.

Typical Particle from Polished $NaNO_3$
Exposed to a Single Pulse at 5.0 J/cm^2

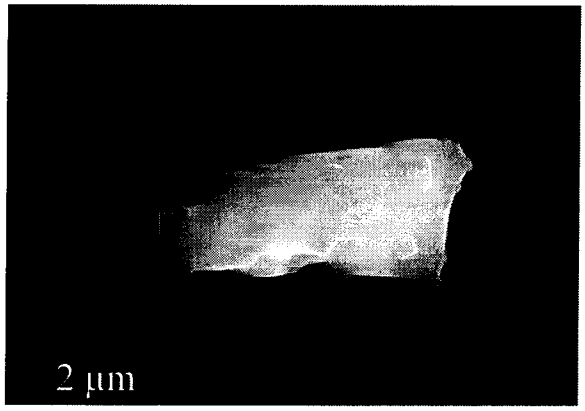

Fig. 9. Angular particle from a polished target exposed to a single pulse at a fluence of 5.0 J/cm^2 showing an extensive halo of nanoparticles. The surface of this particle also shows several crystalline patches, presumably due to aggregation with smaller crystalline particles.

Images of particles collected on a filter membrane during exposure to about 1500 laser pulses at the somewhat higher fluence of 6 J/cm^2 appear in Fig. 10. At this fluence, both cleaved and polished targets yield large numbers of fractured particles [Fig. 10(a)] as well as melted, spherical particles [Fig. 10(b)]. Many of the melted particles appear to be aggregates of smaller particles. In previous work, we measured significant electrical charges of both signs on somewhat larger particles produced during the laser ablation of sodium nitrate at 10 J/cm^2 in a Millikan oil-drop apparatus.[14] The variation of total charge as a function of particle size suggests that the average surface charge densities are fairly consistent. Particles with opposite charge would tend to aggregate, as observed. Strategies to minimize aggregation must account for this charge.

Fluences sufficient to melt the target surface typically produce nanometer-scale particles similar to the halo particles in Figs. 8(b) and 9. When collected on a filter membrane, these nanoparticles typically aggregate into long chains, shown in Fig. 11. These particles were generated at a somewhat lower fluence of about 4 J/cm^2. Chain-like nanoparticle aggregates are frequently observed in a wide variety of contexts, including laser ablation.[17] Aggregation is attributed to electrostatic effects.[18]

4. Discussion

The use of IR radiation instead of the shorter UV wavelengths represents a departure from conventional wisdom regarding laser ablation for analysis. In many materials systems, irradiation at UV wavelengths produces smaller particles which yield superior analytical results.[11,13] Our strategy is to take advantage of the strong thermal stresses generated at IR wavelengths, but to limit the fluence so as to minimize melting and thermal decomposition. This strategy is probably not useful in sample types where thermal effects are not an important source of variability. However, laser-induced fracture may significantly improve analysis in brittle, low melting point crystalline solids that display especially strong thermal effects.

Particles Collected on Filter during IR Irradiation at ~ 6 J/cm^2

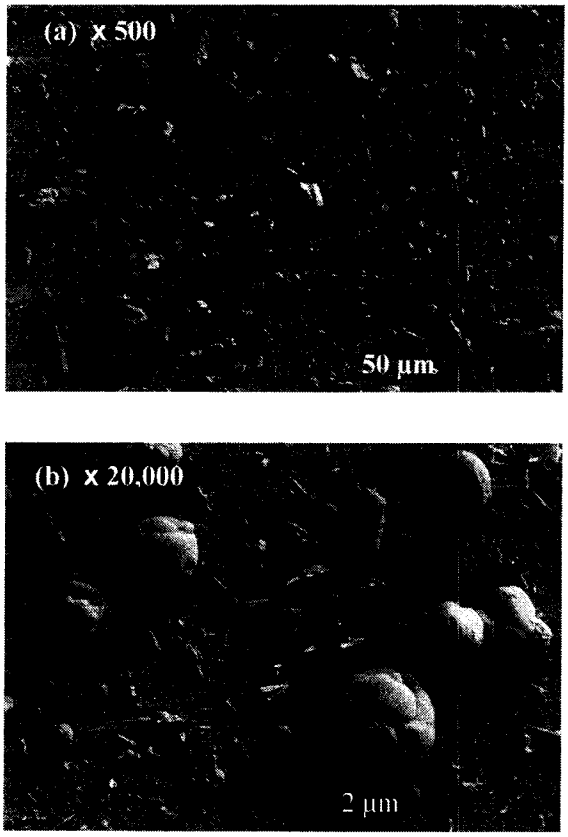

Fig. 10. Filamentary nanoparticle aggregrates collected on a filter membrane during repeated irradiation (about 1500 laser pulses) at a fluence of about 4 J/cm^2.

Filamentary Nanoparticle Aggregates Collected On a Filter during IR Irradiation at ~ 4 J/cm^2

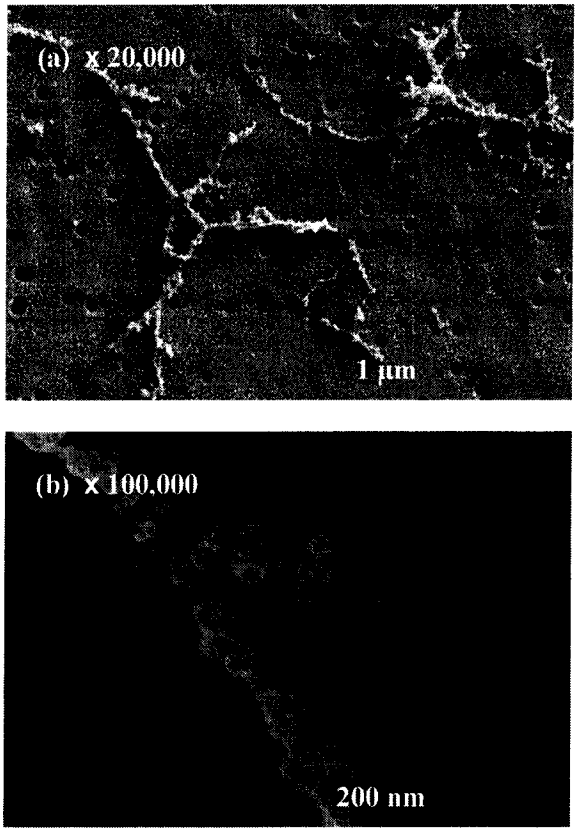

Fig. 11. Particles collected on nucleopore filter during repeated irradiation at a fluence of about 6 J/cm^2: (a) Image at low magnification showing large fracture particles and numerous melted particles and (b) image taken at higher magnification showing aggregates of melted particles as well as smaller melted particles.

Pulsed lasers have long been employed as a source of shock waves for the investigation of spallation phenomenon. Most recently, laser-induced shocks have been employed to study the nucleation, growth, and coalescence of cracks in brittle materials.[19,20] Laser-induced fracture has also been extensively studied as a damage mechanism in optical materials.[21-23] However, the production of particles small enough for ICP-MS applications (0.2 μm–2 μm in diameter) has received little attention.

Crystalline $NaNO_3$ is highly transparent at 1.06 μm, so that the great majority of laser radiation passes cleanly through the sample. The small amount of radiation that is absorbed can still generate substantial radial stresses perpendicular to the laser beam. Bullough and Gilman calculated that tensile stresses produced by a short laser pulse with uniform intensity distribution ("flat topped" beam profile) diverge in the center of the laser spot as the "relation wave"

propagates inward from the edge of the laser spot.[3] Further, these tensile stresses exceed the compressive stress in the irradiated material during the laser pulse over a substantial area—about 20% of the laser spot radius. At low fluences, this tensile pressure will not be sufficient to fracture the bulk material. However, damaged regions of the crystal, especially cleavage steps, are especially vulnerable to such stresses and can fracture off.

Cleavage steps are especially vulnerable to laser-induced damage.[4] Even residual steps on mechano-chemically polished material can substantially lower the fluence required for damage.[5] In some cases, cleavage induced deformation can produce laser-absorbing point defects along steps,[6] increasing the laser induced thermal stresses, and directly resulting in fracture. In the case of MgO, this absorption is attributed to F-centers and F-center clusters which strongly absorb at 248 nm—the wavelength of the KrF excimer.[4] It is not clear that similar defects in $NaNO_3$ might enhance absorption at 1.06 μm. However, it is possible that laser energy scattered of steps and their associated internal interfaces can locally enhance the laser energy density and result in similar heating and fracture. In low-index materials such as $NaNO_3$, Bloembergen estimates that scattering at cracks and pores in a somewhat different geometry can reduced the fluence required for damage by a factor of 2-5.[7] This is broadly consistent with our results, where the threshold for damage of polished samples lies between 3.4 and 5.0 J/cm^2, while cleaved samples are damaged at 3.4 J/cm^2.

5. Conclusions

We have shown that laser-induced fracture along cleavage steps can produced cleavage particles of an appropriate size for ICP-MS analysis at fluences low enough to preclude target or particle melting. The threshold fluence for the onset of melt features on particle and target surface at 1064 nm appears to coincide with the onset of optical breakdown—which in air is accompanied by an audible crack. Although most of the results in this work involve particles produced during the first pulse incident on freshly cleaved surfaces, continued irradiation continues to produce particles, albeit at a reduced rate. Particle aggregation during transport is observed, presumably due to electrostatically charged fragments.

At laser fluences above the threshold for optical breakdown, the target surface and the resulting particles show extensive melt features. Cleavage target surfaces yielded large melted droplets, possibly due to the melting and ejection of cleavage debris. Fractured particles are produced at higher fluences, but the surfaces of these particles are extensively melted. Extensive aggregation is observed, both among particles collected on substrates and particles transported under ICP-MS-like conditions. Nanometer-scale particles are also observed, often forming web-like aggregates during transport. These nanoparticles apparently form by condensation from vapor. Nanoparticles collected on filter membranes may have nucleated in air, but similar particles organized into halo structures around larger, melted particles on collection substrates appear to have nucleated on the substrate. The role of surfaces in nanoparticle nucleation is an interesting question for further study.

Previous work with sodium nitrate and ongoing work with glass samples suggest that both target and particle composition can be strongly affected at temperatures sufficient to cause melting. In the accompanying work, we show that particle production by fracture of cleaved, single crystal material can be sufficient for chemical analysis by ICP-MS, and that repeated exposure to laser fluences sufficient for fracture and not melting does not alter the target

composition as much as higher fluences. For practical applications, more efficient generation of smaller fracture particles is desired.

Acknowledgments

We thank Mary Dawes, Washington State University, for performing the lower resolution SEM work. The high resolution SEM work was performed at Pacific Northwest Laboratory's Environmental Molecular Science Laboratory (EMSL), a national scientific user facility sponsored by the Department of Energy's Office of Biological and Environmental Research. This work was support by the Department of Energy under Grant DE-FG07-97ER62516.

Appendix 2

Matrix effects in the analysis of doped single crystal $NaNO_3$ by laser ablation, inductively couple plasma mass spectroscopy (draft)

S. C. Langford,* A. Mendoza,† M. L. Alexander,† and J. T. Dickinson*

*Physics Department, Washington State University, Pullman, WA 99164-2814
†Pacific Northwest Laboratory, P.O. Box 999, Richland, WA 99352

We compare matrix effects associated with ICP-MS analysis of particles produced by laser ablation single crystal $NaNO_3$ doped with $Sr(NO_3)_2$ and $CsNO_3$ under three laser conditions: high power density UV (355 nm), high power density IR (1064 nm), and low power density IR (1064 nm). The low power density IR conditions were chosen to maximize localized fracture while avoiding optical breakdown at the surface. Under high power density UV irradiation, $NaNO_3$ displays significant incubation-the laser interaction becomes stronger with exposure time-and Cs-depletion is observed. Under high power density IR irradiation, Cs-depletion is observed without apparent incubation. Under low power density IR irradiation, depletion is not observed; however, particle production for analysis depends on the presence of cleavage steps and thus may under-sample regions without cleavage steps. Strategies which maximize fracture may have significant benefits in the analysis of brittle, low-melting point materials, where thermal effects strongly effect the results of analysis.

1. Introduction

Inductively coupled plasma mass spectroscopy (ICP-MS) is a sensitive technique for elemental analysis. Although samples to be analyzed are conventionally delivered to the plasma torch as aqueous solution, samples delivered as small solid particulates (< 2 μm in diameter) can also be analyzed. The resulting reduction in sample handling and waste volume can significantly improve the safety and cost of analyzing hazardous materials. Solid sampling can also facilitate the analysis of small regions in inhomogeneous samples (e.g., mineral grains in geologic samples), yielding information on the range of compositions rather than just an average. Laser-ablation has been successfully employed to provide particles for subsequent ICP-MS. Nevertheless, significant questions remain as to the chemistry of solid particles produced by laser ablation relative to that of the analyte.[10-13]

Sodium nitrate is a major component of high level waste from cold war plutonium production operations in the United States. The small sample sizes and minimal sample handling required by laser ablation ICP-MS are extremely attractive for the analysis of high level wastes. However, $NaNO_3$ displays strong induction under UV radiation-that is, defects produced by UV radiation strongly enhance subsequent UV absorption.[24] Particles produced by laser irradiation also readily decompose to the refractory oxide, Na_2O_2,[14] which is not easily vaporized in the ICP torch. Further, the low melting point of $NaNO_3$ (T_m = 307 °C) and the apparent volatility of

many impurities of interest make it difficult to produce particles of a consistent composition relative to the host.

In this work, we explore some of the relevant matrix effects associated with $NaNO_3$ in a relatively controlled environment, using single crystals doped with impurity cations, such as Sr and Cs. We demonstrate that 355-nm laser radiation produces substantial induction effects, with ICP-MS signals increasing strongly in the early stages of exposure. During the course of irradiation, depletion of volatile components, such as Cs, is also observed. At comparable laser power densities, using 1064-nm radiation reduces incubation effects but aggravates Cs depletion. We report initial work with low power density 1064 nm radiation (raising the laser spot size to produce sufficient particles). Under these conditions, incubation effects and Cs depletion are minimized. At the lowest laser power densities, particle production requires mechanical defects, such as cleavage steps,[1] which in some cases may lead to nonrepresentative sampling. Laser power densities that produce extensive fracture while minimizing surface heating may prove optimum for brittle, low melting point, crystalline matricies such as sodium nitrate.

2. Experiment

Single crystal $NaNO_3$ doped with $Sr(NO_3)_2$ (nominally 1-1000 ppm mole fraction) and $CsNO_3$ (nominally 100 ppm mole fraction) was prepared by slowly cooling (1 °C/hour) molten material in a round-bottom flask. One series of samples was doped with $Mg(NO_3)_2$, $Sr(NO_3)_2$, and $Ba(NO_3)_2$ in comparable concentrations. Laser ablation- and solution-based ICP-MS of the resulting material show strong impurity enhancements along the outer surface of each boule. Thus the local dopant concentrations in samples cleaved from the interior of these boules often contrasted markedly with the nominal sample concentration.

Samples were cleaved from the resulting boules and mounted on a soda lime glass microscope slide in a particle collection chamber equipped with a transparent quartz cover and a beam stop. A Continuum Surelight Nd:YAG laser provided 7 ns pulses of radiation at 1064 and 355 nm. Particles formed by laser irradiation were entrained in flowing argon and transported to a Fissons Instruments VG Plasma Quad PQ2+ STE ICP-MS unit. The MS detector was operated in the pulse counting mode.

A typical experimental run commenced with 60 s of data acquisition without laser exposure to establish a background. Then one of several standard waste glass samples was exposed to the laser for 120 s (6 mJ IR or 1.6 mJ UV) at the focal point of an f = 100 mm lens. Finally, the signal from the $NaNO_3$ sample was acquired for about 400 s, with the laser beam rastering a 5×5 mm^2 square 2-4 times at a pulse repetition rate of 20 Hz. In all cases, the Na signals saturated the detector and are not reported below. Data were acquired under three conditions of laser exposure, chosen to provide appropriate particle densities at the ICP-MS:

An independent estimate of the number and size of particles produced by laser ablation was provided by sampling the Ar flow with a Particle Monitoring System Lasair 1001-(6) particle analyzer. This instrument utilizes scattered laser light to count particles with diameters in the 0.1-2.0 μm range. These measurements were made simultaneously with the ICP-MS analysis. Although the particles entering the size analysis system were not the same particles being analyzed by the ICP-MS, they are believed to be a representative of the particles being analyzed. The total particle volume sampled by the particle monitoring system was estimated by multiplying the number of particles counted in each size bin by the volume of an average particle in that bin.

3. Results

Dopant Distribution. The distribution of Sr and Cs in $NaNO_3$ formed under these conditions is far from uniform. An indication of the spatial distribution of Sr and Cs in the nitrate crystal is given by cleaving the boule across the middle and sampling the composition along a line through the center of the resulting slice. Figure 1 shows the Sr and Cs signals from analysis of particles formed my scanning the UV laser beam (355 nm, 20 J/cm^2) across the center of a slice from a $NaNO_3$ sample doped with nominal 1000 mole-ppm $Sr(NO_3)_2$ and 100 mole-ppm $CsNO_3$. Much of the Sr and most of the Cs is concentrated near the outer edge of the boule-presumably due to the rejection of impurity atoms from the solidifying $NaNO_3$ during crystal growth. Along the scanned line, the count rates for Cs vary by a factor of 80 and the count rates for Sr varies by a factor of 8 variation . Cs is more efficiently segregated than Sr due to the relatively good match between the ionic radii of Na and Sr (R_{Na} = 0.97 Å, R_{Sr} = 1.12 Å, R_{Cs} = 1.67 Å).

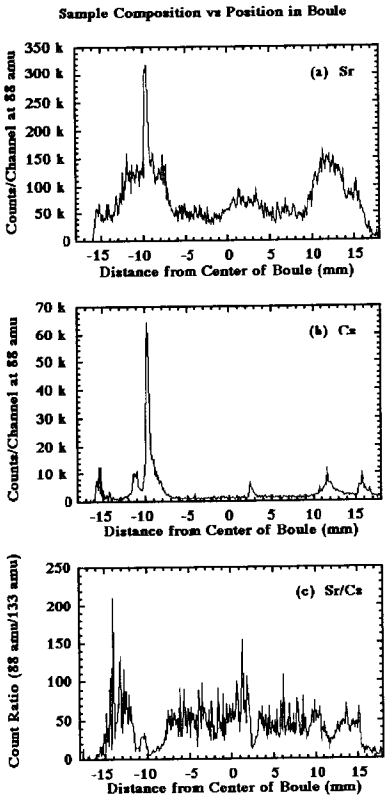

FIG 1. Pulse counted ICP-MS signal intensities at (a) 88 amu (^{88}Sr), (b) 133 amu (^{133}Cs), and (c) the ratio of the 88 amu signal to the 133 amu signal as a 355-nm laser is scanned across a cross-section of a $NaNO_3$ boule. The boule was doped with 1000 ppm Sr and 100 ppm Cs (nominal concentrations).

The Sr/Cs count ratio appears in Fig. 1(c). Although the Sr/Cs ratio is relatively constant throughout much of the interior, patches of high Cs concentration are associated with order-of-magnitude drops in the ratio of Sr/Cs ratio. These variations complicate comparisons between signals observed under different laser conditions at different positions along the sample. The

ratio of total Sr counts to total Cs counts (background subtracted) along the entire scan is 22—about double the ratio of 10 expected on the basis of the nominal composition.

High Power Density UV. In terms of variability, the best results for a many materials are obtained in the UV. Most materials absorb strongly in the UV, concentrating the laser energy near the surface for efficient particle production while minimizing thermal effects. Figure 2 shows Sr and Cs signals as the UV laser (355 nm—20 J/cm^2) samples both a glass standard (CVS16) and a doped $NaNO_3$ sample (nominally 30 mole ppm Sr, 100 mole ppm Cs). With each 150 s scan, both the Sr and Cs signals increase. This step wise increase with each scan is especially dramatic in the Sr signal. We attribute the rise in Sr and Cs signals to increased laser absorption accompanying UV-induced defect production (i.e., incubation), which is readily observed in this material.[24] Similar defects are produced by other ionizing radiations,[25] including those expected in radiological wastes. Significantly, the Sr/Cs signal ratio rises from scan to scan, from 4.8 during the first scan to about 20 in the last scan. This is consistent with Cs depletion due to generalized sample heating. Incubation and depletion of volatile components complicate the analysis of low melting point, radiation-sensitive materials like $NaNO_3$ under UV radiation.

Under high power density UV irradiation [Fig. 2(d)], the total volume of sampled particles increases throughout data collection, consistent with the induction process implied in the ICP-MS signals. Changes in particle volume are generally tracked by the Sr, but some depletion in the Cs signal is apparent. In contrast to IR irradiation (regardless of power density), particle production in the UV show little variation within a given scan. Thus particle production in the UV was relatively unaffected by local variations in surface condition. SEM examination of particles collected on filter paper showed a large number of μm-sized and smaller melted spheres. Condensation from vaporized material appears to be a major particle production mechanism.

High Power Density IR. Sr and Cs signals obtained under high power density IR irradiation (1064 nm—75 J/cm^2) of this same sample appears in Fig. 3. Here the scan duration has been shortened to about 100 s. No significant change in the Sr and Cs signals or their ratio appears from one scan to the next. Some samples showed factor-of-two variations in Sr and Cs signals that reproduced from scan to scan and correlated with the instantaneous rate of particle production, discussed below. Point-to-point variations in IR absorption apparently alter particle production in a reproducible way as the same region is scanned 4-5 times. The Sr/Cs signal ratio in Fig. 3(c) is about 2.5 for each of the three scans across the irradiated regions.

High density IR radiation [Fig. 3(d)] produces an enormous particle volume that grows over the first 30 s or so and then plateaus. Interestingly, the rate of particle production increases during the short interval where the Sr/Cs signal ratio increases dramatically. Several samples showed marked variations in particle volume as the laser scanned the surface. These changes were reproduced from scan to scan and were also reflected in the Sr and Cs signals. SEM observations of particles collected on filter paper showed large numbers of μm-sized fractured and melted particles.

Low Power Density IR. At low power densities, thermal effects should be minimal, but particle generation is generally confined to surface defects such as steps. Sufficient particle generation for analysis can be achieved with cleaved $NaNO_3$ at an average fluence of 3.4 J/cm^2 with a laser spot about 2.3 mm in diameter. The resulting Sr and Cs signals from a sample with the same nominal composition as those in Figs. 2 and 3 are shown in Fig. 4. The Sr and Cs signals during the first 100 s scan are much more intense than the subsequent scans due to the

large volume of particles produced during the first scan. The signals produced during the second and subsequent scans are much more uniform. The Sr and Cs signals vary from point-to-point within each scan, but these variations are consistent from scan to scan. The Sr/Cs ratio is about 0.16 for the initial scan across the surface, and changes little during subsequent scans.

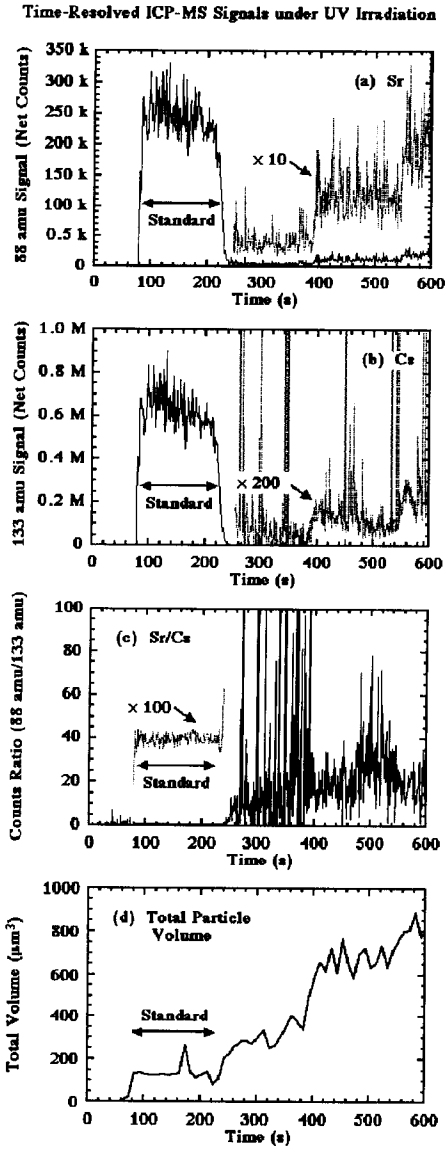

FIG. 2. Pulse counted ICP-MS signal intensities at (a) 88 amu (^{88}Sr), (b) 133 amu (^{133}Cs), (c) the ratio of the 88 amu signal to the 133 amu signal, and (d) total particle volume in a sampled fraction of Ar as a 355-nm laser is ratered over a glass standard and a doped $NaNO_3$ boule. The boule was doped with 30 ppm Sr and 100 ppm Cs (nominal concentrations).

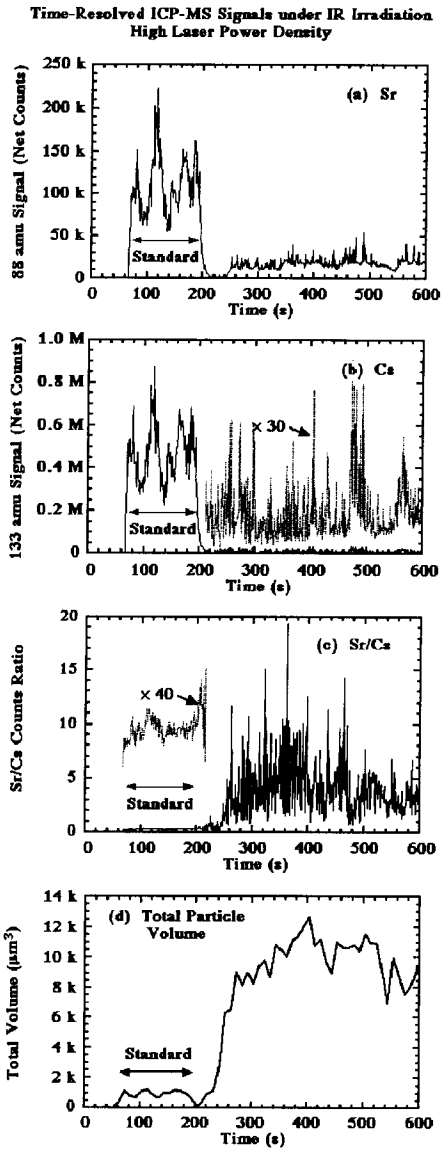

FIG. 3. Pulse counted ICP-MS signals at (a) 88 amu (^{88}Sr), (b) 133 amu (^{133}Cs), (c) the ratio of the 88 amu signal to the 133 amu signal, and (d) total particle volume in a sampled fraction of Ar as a 1064-nm laser is rastered over a glass standard and a doped $NaNO_3$ crystal (30 ppm Sr, 100 ppm Cs nominal). The sample surface was located at the focal point, yielding a high power density at the surface.

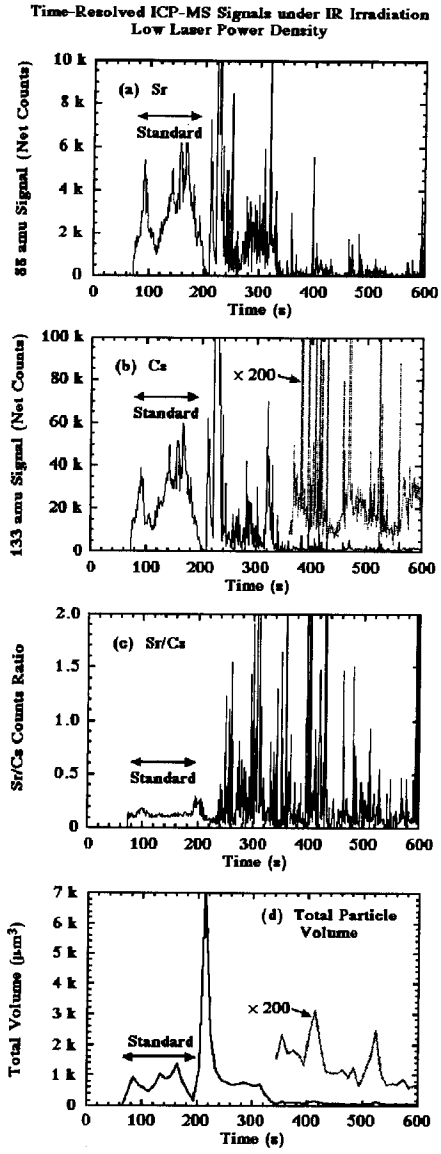

FIG. 4. Time-resolved ICP-MS signals at (a) 88 amu (^{88}Sr), (b) 133 amu (^{133}Cs), (c) the ratio of the 88 amu signal to the 133 amu signal, and (d) total particle volume in a sampled fraction of Ar as a 1064 nm laser is rastered over a glass standard and a doped $NaNO_3$ crystal (30 ppm Sr, 100 ppm Cs nominal). The sample surface was offset about 12 mm from the focal point, yielding a low power density at the surface.

The low power density irradiation typically yields a large spike in total volume immediately after the laser is positioned onto the $NaNO_3$, consistent with the large spike in the Sr and Cs signals. We attribute this to laser-induced fracture of the most vulnerable cleavage steps, not only in the laser spot but also in nearby material.[1] This accounts for the marked decrease in particle production throughout the remainder of the first scan. Nevertheless, this reduced level of particle production is exceeds that of subsequent scans, consistent with the removal of additional loosely bound material. Point-to-point variations in particle production are common and reproducible from scan to scan; more particles are produced when the laser crosses regions of the sample with especially favorable cleavage steps for particle production .

Particle Composition. As the sample composition along the surface often varied by factors of ten or more at points one mm apart, comparisons between particle composition by ICP-MS versus target composition were not reliable. Nevertheless, it is instructive to compare the integrated impurity mass signals during line scans across the entire boule with the nominal boule composition. Although this procedure is still not entirely representative, the trends in measured composition illustrate the issues associated with particle production by laser ablation under each condition. The samples employed in this work were doped with 100 atomic ppm $Mg(NO_3)_2$, and with various concentrations of $Sr(NO_3)_2$, and $Ba(NO_3)_2$. As in the work above, the best lattice match with $NaNO_3$ is achieved with $Sr(NO_3)_2$, so that thermal effects with Sr are expected to be smaller than with Mg and Ba. In each case, the laser was scanned across the sample at a rate of 5 mm/s, and the ICP-MS scanned through masses appropriate to Mg, Sr, and Ba. At the laser repetition rate employed, each position along the scan line was hit by several overlapping laser pulses. The total counts for each of the majority masses corresponding the Mg, Sr, and Ba were summed, and the fraction of the total counts due to each of the minority species computed. The fluences under each condition were somewhat lower than in the work reported above. The results of this analysis for two boules with contrasting compositions appear in Table 2. The most obvious trends are observed with the majority components, where any distortion in sampling and analysis will be less affected by the distortions in the other components.

High power density UV scan (355 nm—3.8 J/cm^2) severely under-represents the amount of Mg in the sample with 0.224 Mg fraction and significantly under-represents the amount of Ba in the sample with 0.907 Ba fraction. In contrast, the Sr fraction is over-reported in both samples. These results are consistent with depletion of Mg and Ba relative to Sr, similar to the depletion of Cs relative to Sr described above.

Table 1. Background corrected impurity count fractions for two doped $NaNO_3$ samples

Mass	Dopant Levels	UV High	IR High	IR Low	Nominal
24 amu	100 ppm	0.041	0.205	0.754	0.224
88 amu	300 ppm	0.895	0.688	0.131	0.732
138 amu	10 ppm	0.064	0.106	0.116	0.024
24 amu	100 ppm	0.247	0.042	0.509	0.091
88 amu	3 ppm	0.009	0.011	0.077	0.003
138 amu	1000 ppm	0.744	0.947	0.414	0.907

Overall, the high power density IR laser (1064 nm—30 J/cm^2) yields the best results with the majority impurities, yielding agreement with the nominal concentrations to within about 20% of impurities at nominal concentrations greater than 200 ppm. This fluence is less than half the fluence employed in the Cs-doped material described above, which may account for the minimal depletion observed in the total counts summed along the line scan. Moving the laser spot a few millimeters and performing a second scan yielded values about 30% of those reported above. This establishes a crude estimate of the homogeneity of boule as sampled across the boule at along nearby lines. Optical microscopy of the line scans formed by IR laser showed that scanning had formed a deep, fractured trench, tens of microns deep. This extensive material

removal probably allowed for more representative sampling, with less thermally-induced composition change than the other two treatments. It is unlikely that the particle size distribution was particularly suitable for ICP-MS, but this problem appears to be less important than sampling and depletion effects in this intractable materials system.

In both samples, the low power density IR (1064 nm—2.8 J/cm^2) show significant Mg excesses. This counters any trend expected on the basis of impurity segregation. Rastering the low power density beam across the same line yielded very similar results (within 20% at all masses), confirming that any impurity segregation during the first line scan is minimal. We suggest that the Mg excess is due to the effect of impurity aggregates on cleavage. High concentrations of strain inducing impurities (with poor lattice matches, like Mg and Ba) render the material more brittle. Impurity aggregates, which are highly likely, also serve as stress concentrators; approaching cracks are typically attracted to such aggregates. Any impurity aggregates that cause the crack front to rotate out the nominal cleavage plane would be associated with high densities of cleavage steps—features necessary for particle generation at low power densities. Thus certain portions of the sample would be selectively sampled (here, regions with excess Mg). Representative sampling at low power densities will require strategies that ensure more uniform sampling.

4. Discussion

Sodium nitrate is a difficult matrix material for analysis by laser ablation ICP-MS. At all three wavelengths, the behavior of the waste glass standard samples was much better for analytical purposes—with no obvious induction or depletion effects. In particular, the variation in the Sr and Cs signals during high power density UV irradiation were small, the variation in the Sr/Cs signal ratios even smaller. Particle production from the waste glass standards were relatively constant during irradiation, especially under UV irradiation. We attribute the relative good behavior of waste glass to its relatively amorphous, open structure, which is less likely to reject impurities upon solidification from the liquid phase or condensation from the vapor. The waste glass is relatively opaque in the UV, so that most of the radiation is absorbed near the surface. Thus surface melting and particle formation by spallation of liquid and condensation of vapor is relatively efficient. Any thermal effects on particle composition should be relatively easy to account for by calibrating with appropriate standards.

The situation with single crystal $NaNO_3$ is much more complex. Phase segregation in the solid is expected to have extreme consequences on the concentrations of impurities in particles formed in the melt or by condensation of vapor. At high impurity concentrations, impurities will form their own phase in the solid. In the case of $NaNO_3$, most of these phases have higher melting points than $NaNO_3$ and thus tend to be under-represented in particles formed by melting or condensation of vapor. The importance of this effect will depend on the fraction of the impurity in phase segregated crystallites and their melting point relative to $NaNO_3$ and crystallites incorporating other impurities. In the absence of superheating, the laser-induced melt may never exceed the melting point of impurity phases, potentially exacerbating the depletion of impurities in the ejected material.

Impurities which are dispersed in the $NaNO_3$ matrix are much more likely to incorporated into melted particles stoichiometrically, although there is some question about the fate of impurity vapors. Little work has been done on how minority species in vapors interact with particles condensed of the majority phase. Molecular species that are not incorporated into

particles are likely to diffuse to and absorb along the walls of tubing. Simplistically, one also expects impurities dispersed in the $NaNO_3$ matrix to lower the melting point of the matrix in much the same way that impurities in water lower its freezing point. The ease with which impurities are volatilized will depend strongly on the impurity.

All of these effects depend strongly on the thermal history of the material incorporated into the analyzed particles, and thus on the particle generation mechanism. Extreme thermal effects are possible in particles condensed from vapor, while smaller thermal effects are expected in particles spalled from the surface in liquid form. Ideally, thermal effects could be further minimized by laser-induced fracture.

Our attempts to produce particles by fracture initially focused on low power densities, power densities below the threshold for optical breakdown. Optical breakdown invariably melts the surface and thermally processes the material. As shown in Appendix 1, fracture under these conditions is localized to vulnerable material along cleavage steps. In the presence of high impurity concentrations, such targets are not uniformly sampled. As suggested above, the composition of the resulting particles can be unrepresentative of the whole. In retrospect, it appears that fluences above the threshold for optical breakdown (here, about 30 J/cm^2 at 1064 nm) can generate large amounts of fractured particles without large thermal changes in the average particle composition. Observations in Appendix 1 suggest that many of these particles will experience at least superficial melting. At sufficiently high fluences (here, 75 J/cm^2 at 1064 nm), we observe large thermal effects on particle composition. This suggests that a window of fluences at 1064 nm can be found for doped-$NaNO_3$ for which thermal effects on particle composition are manageable, and that particle composition is reasonably close to that of the target.

We emphasize that the goal of matching particle composition to target composition is not necessarily appropriate for all samples. For analytical purposes, matrix effects in more well-behaved materials can often be accounted for by using a range of appropriate standards. When matrix effects are not the principal source of analytic uncertainty, optimum particle production for analysis may well require melting and/or vaporizing the target material. In the case of doped $NaNO_3$, matrix effects are severe and are not easily corrected on the basis of standard samples. Our efforts to produce well characterized, doped single crystal standards consistently failed, although amorphous or highly polycrystalline standards may yet prove viable. In this brittle materials system, analysis by LA/ICP-MS may be improved by choosing laser conditions that generate copious amounts of fracture particles that minimize the need for such corrections.

4. Conclusions

ICP-MS and particle-size analysis of doped $NaNO_3$ is complicated by the inhomogeneous composition of crystalline samples and strong thermal effects that selectively deplete some impurity components over others in a complicated fashion. The interaction of $NaNO_3$ with UV radiation depends strongly previous exposure to UV and other ionizing radiation, with significant effects on the rate of particle production. Particles produced by focused UV lasers at modest and high power densities (fluences > 3 J/cm^2) are depleted in some impurity components in a history and composition dependent way. Similar, complex depletion effects were observed under high power density IR irradiation (> 60 J/cm^2). Attempts to produce more suitable particles by lowering the IR power density below the threshold for optical breakdown provided more consistent analyses, but the resulting particles are often generated

from a relatively small and probably unrepresentative fraction of the surface associated with cleavage steps. Preliminary results suggest that IR radiation at power densities corresponding to about 30 J/cm^2 can produce copious particles for analysis whose composition approaches that of the sample. Many of these particles undoubtedly are melted, but the resulting thermal effects on particle composition are not excessive for the tested ionic impurities at the 100 ppm level or greater. Further work is clearly advised.

Acknowledgments

This work was support by the U.S. Department of Energy under Grant DE-FG07-97ER62516.

Appendix 3.

Mechanisms of particle generation in laser ablation of solid materials for inductively coupled plasma mass spectrometer (ICP/MS) (abstract)

Michael L. Alexander,† Albert Mendoza,† Amanda L. Hedges,† J. Thomas Dickinson* and Stephen C. Langford*

†Pacific Northwest Laboratory, P.O. Box 999, Richland, WA 99352
*Physics Department, Washington State University, Pullman, WA 99164-2814

Laser ablation inductively coupled plasma mass spectroscopy (LA/ICP-MS) has gained increasing acceptance as valuable method for the rapid chemical analysis of solid material. The LA/ICP-MS method utilizes particles generated by laser ablation of solid material for subsequent elemental analysis. The accuracy of the method depends on how well the composition of the particulates reflects the sample under investigation, transport to the plasma and quantitative digestion in the ICP. We present the results of research that illuminates the physical mechanisms involved in laser ablation generation of particulates for subsequent ICP/MS analysis. Particles were collected from laser ablation of samples possessing a variety of physical properties including thermal conductivity, melting point, heat capacity, and optical absorption. Sample matrix types included amorphous glasses single crystals, metals and aggregated particulates. Laser ablation wavelength was varied from 1900 to 266 nm, pulse lengths were from 10 ns to 20 ps, pulse energies ranged from 10 μJ/pulse to 10 mJ/pulse in a spot size from 50 to 500 microns. Particles were collected on a filter and analyzed by scanning electron microscopy (SEM) and energy dispersive x-ray spectroscopy (EDX). Several classes of ablated particles were identified and analyzed for composition. Models are presented for the formation mechanisms of these particles based on thermal and optical properties of the sample material.

Appendix 4. Literature Cited

1. S. C. Langford, J. T. Dickinson, and M. L. Alexander, "The production of sub-micron sodium nitrate particles by laser ablation," Appl. Phys. A **69,** S647-S650 (1999).
2. S. C. Langford, M. L. Alexander, J. S. Young, and J. T. Dickinson, "Production of particles by laser-induced fracture of single crystal $NaNO_3$ for chemical analysis by inductively coupled mass spectroscopy," manuscript in preparation (2001).
3. R. Bullough and J. J. Gilman, "Elastic explosions in solids caused by radiation," J. Appl. Phys. **37,** 2283-2287 (1966).
4. J. T. Dickinson, L. C. Jensen, R. L. Webb, M. L. Dawes, and S. C. Langford, "Interactions of wide band gap single crystals with 248 nm excimer laser radiation. III. The role of cleavage-induced defects in MgO," J. Appl. Phys. **74,** 3758-3767 (1993).
5. E. Stenzel, S. Gogoll, J. Sils, M. Huisinga, H. Johansen, G. Kästner, M. Reichling, and E. Matthias, "Laser damage of alkaline-earth fluorides at 248 nm and the influence of polishing grades," Appl. Surf. Sci. **109-110,** 162 (1997).
6. J. T. Dickinson, L. C. Jensen, R. L. Webb, and S. C. Langford, "Photoluminescence imaging of mechanically produced defects in MgO," J. Non-Cryst. Solids **177,** 1-8 (1994).
7. N. Bloembergen, "Role of cracks, pores, and absorbing inclusions on laser induced damage threshold at surfaces of transparent dielectrics," Appl. Opt. **12,** 661-664 (1973).
8. S. C. Langford, J. T. Dickinson, A. Mendoza, and M. L. Alexander, "Matrix effects in the analysis of doped single crystal $NaNO_3$ by laser ablation, inductively couple plasma mass spectroscopy," manuscript in preparation (2001).
9. M. L. Alexander, A. Mendoza, A. L. Hedges, S. C. Langford, and J. T. Dickinson, "Mechanisms of particle generation in laser ablation of solid materials for inductively coupled plasma mass spectrometer (ICP-MS)," manuscript in preparation (2001).
10. W. T. Chan and R. E. Russo, "Study of laser-material interactions using inductively coupled plasma-atomic emission spectrometry," Spectrochim. Acta B **46,** 1471-1486 (1991).
11. M. L. Alexander, M. R. Smith, T. L. Stewart, and J. S. Hartman, "FY1994 Year-End Technical Letter Report: Laboratory Demonstration System, Development, and Laboratory LA/MS Testing Activity," Report No. PNL Project 19928-05 (1994).
12. R. E. Russo, X. L. Mao, M. Caetano, and M. A. Shannon, "Fundamental characteristics of laser-material interactions (ablation) in nobel gases at atmospheric pressure using inductively coupled plasma-atomic emission spectroscopy," Appl. Surf. Sci. **96-98,** 144-148 (1996).
13. D. Figg and M. S. Kahr, "Elemental fractionation of glass under laser ablation inductively coupled plasma mass spectroscopy," Appl. Spectroscopy **51,** 1185-1192 (1997).
14. R. L. Webb, J. T. Dickinson, and G. Exarhos, "Characterization of particulates accompanying laser ablation of $NaNO_3$," Appl. Spectrosc. **51,** 707-717 (1997).
15. M. V. Swain, B. R. Lawn, and S. J. Burns, "Cleavage step deformation in brittle solids," J. Mater. Sci. **9,** 175-183 (1974).

16. S. J. Pennycook and L. M. Brown, "Cathodoluminescence at dislocations in divalent oxides," J. Lumin. **18/19,** 905-909 (1979).

17. M. S. El-Shall, S. Li, T. Turkki, D. Graiver, U. C. Pernisz, and M. I. Baraton, "Synthesis and photoluminescence of weblike agglomeration of silica nanoparticles," J. Phys. Chem. **99,** 17805-17809 (1995).

18. T. B. Jones, *Electromechanics of Particles* (Cambridge University, Cambridge, 1995).

19. T. d. Rességuir and F. Cottet, "Experimental and numerical study of laser induced spallation in glass," J. Appl. Phys. **77,** 3756-3761 (1995).

20. X.-Z. Li, M. Nakano, Y. Yamauchi, K. Kishida, and K. A. Tanaka, "Microcracks, spall and fracture in glass: A study using short pulsed laser shock waves," J. Appl. Phys. **83,** 3583-3594 (1998).

21. N. Bloembergen, "Laser-induced electric breakdown in solids," IEEE J. Quantum Electronics **QE-10,** 375-386 (1977).

22. L. L. Chase, A. V. Hamza, and H. W. Lee, in *Laser Ablation—Mechanisms and Applications*, edited by J. C. Miller and R. F. H. Jr. (Springer-Verlag, Berlin, 1991), p. 193-202.

23. B. C. Stuart, M. D. Feit, A. M. Rubenchik, B. W. Shore, and M. D. Perry, "Laser-induced damage in dielectrics with nanosecond to subpicosecond pulses," Phys. Rev. Lett. **74,** 2248-2251 (1995).

24. R. L. Webb, S. C. Langford, and J. T. Dickinson, "Neutral atom and molecule emission accompanying 248-nm laser irradiation of single crystal $NaNO_3$," Nucl. Instrum. Meth. Phys. Res. B **103,** 297-308 (1995).

25. E. R. Johnson, *The Radiation-Induced Decomposition of the Inorganic Molecular Ions* (Gordon and Breach, New York, 1970).